THE ASTROPHYSICAL JOURNAL, 278:486–498, 1984 March 15


# THE ABSORPTION LINE PROFILES IN Q1101−264

ROBERT F. CARSWELL
Institute of Astronomy, Cambridge
DONALD C. MORTON
Anglo-Australian Observatory
MALCOLM G. SMITH
Royal Observatory, Edinburgh
ALAN N. STOCKTON
Institute for Astronomy, University of Hawaii
AND
DAVID A. TURNSHEK AND RAY J. WEYMANN[1]
Steward Observatory, University of Arizona
*Received 1983 June 7; accepted 1983 August 25*

## ABSTRACT

Three regions of the spectrum of the bright quasar Q1101−264 have been observed with a resolution of 0.25 Å (FWHM) at the Anglo-Australian Telescope. An absorption redshift system at $z_{abs} = 1.8387$, previously reported as being single, is found to contain at least five components with a total velocity spread of 160 km s$^{-1}$. A new Mg II complex also is present at $z_{abs} = 0.3564$ and 0.3591 with pairs of components separated by 24 and 40 km s$^{-1}$, respectively, and a total range of 630 km s$^{-1}$. The profiles of the numerous Ly$\alpha$ lines are almost invariably resolved, with velocity dispersion parameters $b = 2^{1/2}\sigma_x$ generally in the range 10–45 km s$^{-1}$ and a range of column densities up to about $10^{15}$ cm$^{-2}$. Some implications of these observations are discussed.

*Subject heading:* quasars

## I. INTRODUCTION

While there may be some exceptions, it appears likely that most of the narrow-line absorption systems seen in quasar spectra are due to intervening galaxies, or intergalactic clouds, on the line of sight to the quasar (e.g., Weymann, Carswell, and Smith 1981). The next step in the study of these systems is to determine, as far as possible, the conditions and abundances in these clouds, and so investigate the less bizarre regions of the universe at high redshifts. From studies of the gas in the halo of our own Galaxy (e.g., York 1982) we know that to make significant progress, high-resolution spectra are required, else the results are confused by blending of lines at different redshifts. Accordingly we have obtained high-resolution spectra of one relatively bright quasar, Q1101−264 with $m_V = 16.1$ and $z_{em} = 2.14$, which was discovered by Osmer and Smith (1977). The absorption line spectrum has been studied at lower resolution by Carswell *et al.* (1982) and Young, Sargent, and Boksenberg (1982). Boksenberg and Snijders (1981) obtained far-ultraviolet spectra which revealed the higher Lyman lines and discontinuity belonging to the system of strong, low-ionization absorption lines at $z_{abs} = 1.8387$ found in the visible spectra. We particularly wished to investigate this system and some of the many lines identified with Ly$\alpha$.

The 1950.0 coordinates of Q1101−264, as measured with the Anglo-Australian Telescope (AAT), are $11^h00^m59^s.8$, $-26°29'08''$. However, to be consistent with earlier published work, we shall retain the designation 1101−264 rather than truncate the AAT value.

[1] Visiting Astronomer, Cerro Tololo Inter-American Observatory, which is supported by the National Science Foundation under contract AST 78-27879.

## II. THE OBSERVATIONAL MATERIAL

Spectra of Q1101−264 at a reciprocal dispersion of 5 Å mm$^{-1}$ were obtained in second order using the Image Photon Counting System (IPCS) with the 82 cm focal length camera on the RGO spectrograph at the Anglo-Australian Telescope. Table 1 gives details of the wavelength regions covered, and the integration times for each of these. The regions were chosen to provide information on absorption lines in the $z_{abs} = 1.8387$ system reported by Carswell *et al.* (1982), in particular to cover the C IV $\lambda\lambda$1548, 1550, Si II $\lambda\lambda$1260, 1304, 1526, O I $\lambda$1302, and C II $\lambda$1334 lines, and to check on the presence of N V $\lambda\lambda$1238, 1242.

The data were recorded in the two-dimensional mode over 1997 channels along the spectrograph dispersion, with each channel corresponding to about 0.07 Å. Along the slit the spectra were recorded in eight increments of approximately 0.″75 each; the object spectrum was recorded in the central three or four of these increments, and the rest contained sky signal alone. The slit width throughout the observations was 0.″4, which gave a measured instrument profile of 0.25 Å (FWHM). The seeing throughout the nights of April 27–30 was exceptionally good, estimated to be about 2/3 arcsec, so, while the light losses at the slit were significant, they were not prohibitive.

In the absence of a suitable filter to exclude contamination of the spectrum by first order light, the short wavelength

TABLE 1

OBSERVATIONS

| Date 1978 April (UT) | Wavelength Range (Å) | Integration Time (s) | Comments |
|---|---|---|---|
| 14.45 | 3680–3820 | 12,000 | BG 38 filter |
| 14.59 | 4306–4440 | 3600 | no filter |
| 27.46 | 4309–4443 | 15,800 | no filter |
| 28.36 | 3690–3829 | 1000 | BG 38 filter |
| 28.46 | 3683–3822 | 13,500 | |
| 30.47 | 3491–3692 | 13,200 | no filter |

region (3490–3630 Å) was observed without any filter at all. The red leak was estimated by obtaining a short integration with a GG495 filter in place, comparing the count rate with that from the unfiltered observation, and subtracting that fraction of the total (about 20%) from the continuum level. Thus there is some uncertainty in the zero intensity level for these data, but the residual intensities of the strong lines appear to be close to zero as we might expect. The spectra are shown in Figure 1.

Data reduction techniques, and the methods used for obtaining continuum levels, absorption line wavelengths and equivalent widths, were identical to those described by Carswell *et al.* (1982). The higher dispersion used here has allowed an unambiguous determination of the continuum using averages over 35 channels as local estimates when there were no deviations outside those expected given the local signal-to-noise ratio. A candidate line was deemed to be real if its equivalent width, $W$, was over 4 times the error due to counting statistics, $\sigma(w)$, determined over the line width. The list of absorption lines selected in this way is given in Table 2. Many of these lines are clearly resolved on our spectra; where component structure is relatively clear, the wavelengths and equivalent widths for the individual components are given. Of course, there may be more component structure on a finer scale, and, since the ability to resolve lines into components depends also on the signal-to-noise ratio, some apparently single features may be multiple. In compiling the line list we have opted to treat doubtful cases as single lines.

Comparison of the wavelengths and equivalent widths of the lines measured here with those determined by Carswell *et al.* (1982) at lower resolution shows, after allowance for unresolved blends in the lower resolution data, no systematic discrepancies. The agreement in equivalent widths between the two sets of observations, and the absence of a forest of very weak lines between those measured on the lower dispersion spectra, suggest that at redshift $z \sim 2$ there is no difficulty in adequately defining the continuum level on 1.5–2 Å resolution data.

Most of the identified lines are those reported by Carswell *et al.* (1982), but the improved wavelength accuracy and ability to intercompare line profiles have enabled us to check and refine some possible identifications. Details of these are discussed in the following sections.

Since many of the lines are clearly resolved without showing signs of velocity substructure, we have been able to fit Voigt profiles and so estimate redshifts, column densities, and velocity dispersion parameters as listed in Table 2. Where identification with a heavy element in a plausible redshift system is not possible, the feature is assumed to be Ly$\alpha$. Note that the mean wavelength given in Table 2 was determined simply from the line centroid, not by profile fitting. Thus it is not necessarily the best estimate for determining a redshift if the line is not symmetric. Therefore the ratio of the vacuum wavelengths, $\lambda_{obs}/\lambda_{lab}$, will not necessarily give the same redshift as the profile fitting method, though it must be very close. All the redshifts given in Table 2 were derived by profile fitting in this way, using the wavelengths and oscillator strengths listed by Morton (1978). Of course, at the resolution of these data it is important to transform all observed and laboratory wavelengths to vacuum values.

For complex features we have fitted a number of Voigt profiles, attempting to fit the minimum number of components to any blend. In some cases this leads to a different decomposition and a different number of components from those obtained by noting the positions of the local maxima and minima within the blend. Where this has occurred is immediately obvious from Table 2, especially where the number of components differs. The method used for fitting the profiles is relatively straightforward. The wavelength limits of the line profiles were determined interactively, and the velocity dispersion parameter ($b = 2^{1/2}\sigma_x$), column density $N$, and redshift $z$ adjusted to minimize the $\chi^2$ calculated using the known photon counting error over the total width of the line. Approximate confidence limits to the three parameters were set by requiring that $\chi^2 = \chi^2_{min} + 3.66$, this last number being chosen to give a confidence level of 70% for three degrees of freedom, so that it is roughly comparable with the $\sigma$ one is familiar with from the normal distribution. However, the error surfaces are not symmetric about the best estimate here, so this analogy should not be taken too far. An illustration for a worst-case strong absorption line showing the shape of the constant confidence limit contours is given in Figure 2. Two points are highlighted in this case. First, the constant error curves can be very asymmetric, and quoted limits at 70% confidence may bear little relation to, for example, the 90% confidence limits. Second, the $\chi^2$ function may have two minima in the log $b$–log $N$ plane, and so there may be some ambiguity in the values chosen. We have opted for the minimum $\chi^2$ in any case where this occurs, and usually the $\chi^2$ value for the other minimum is unacceptably large. For a general discussion of parameter estimation using $\chi^2$ in this way see Lampton, Margon, and Bowyer (1976).

The parameters and error estimates for the blended lines are subject to uncertainty. We have chosen to determine quantities for an individual component in a blend by doing this self-consistently for all lines which make up the overall feature. Thus, the column density, velocity dispersion, and

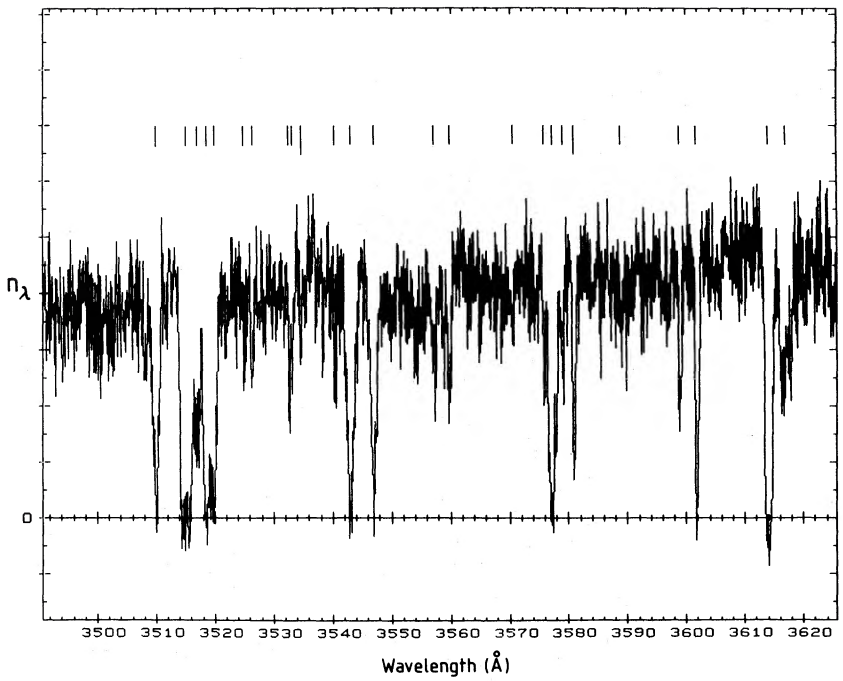


FIG. 1*a*.

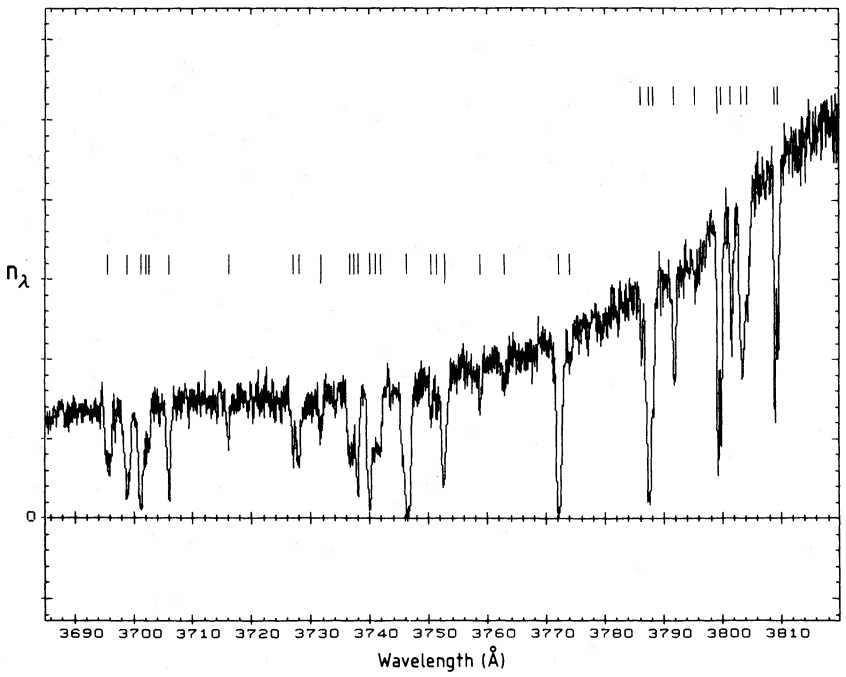


FIG. 1*b*.

FIG. 1.—The spectra of the selected wavelength regions in Q1101 – 264

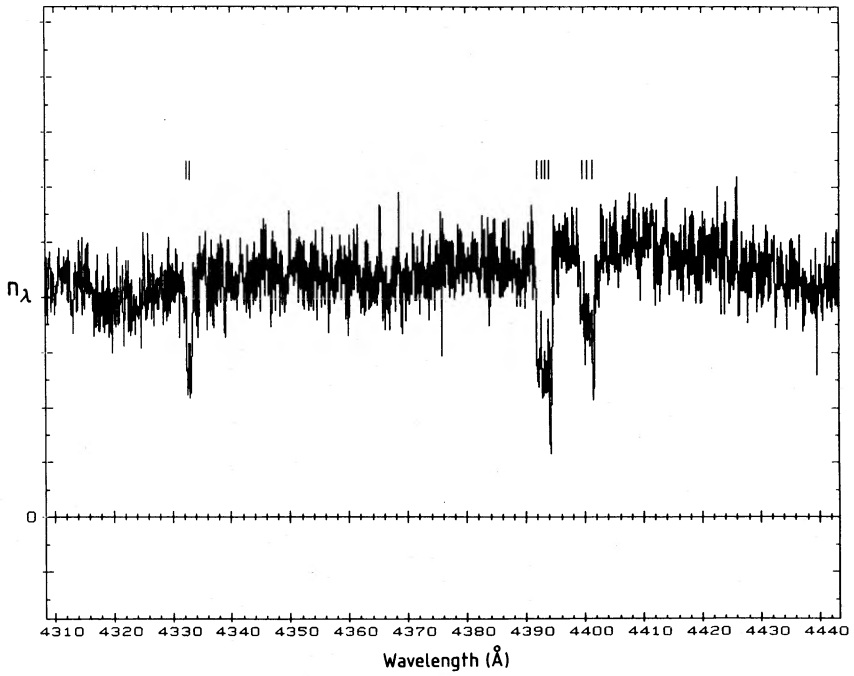


FIG. 1*c*.

redshift ranges for such a line were determined after modifying the local continuum to include the best estimated profiles for the other lines in the blend and do not include any uncertainties introduced from the possible range of values for other components. Features affected in this way are indicated with a vertical bar in the Comments column in Table 2.

Where lines arise from doublets such as Mg II or C IV the velocity dispersions and column densities were determined by minimizing $\chi^2$ simultaneously over both the features. In principle this should have worked for the three lines of Si II at $z_{abs} = 1.8387$ as well, but the analysis here was complicated by the presence of another line (preumably Ly$\alpha$) at the expected positions of the Si II $\lambda$1304 components. An additional problem turned out to be the uncertainty in the Si II oscillator strengths. The contentious one here is Si II $\lambda$1526, for which Morton (1978) gives the experimental value

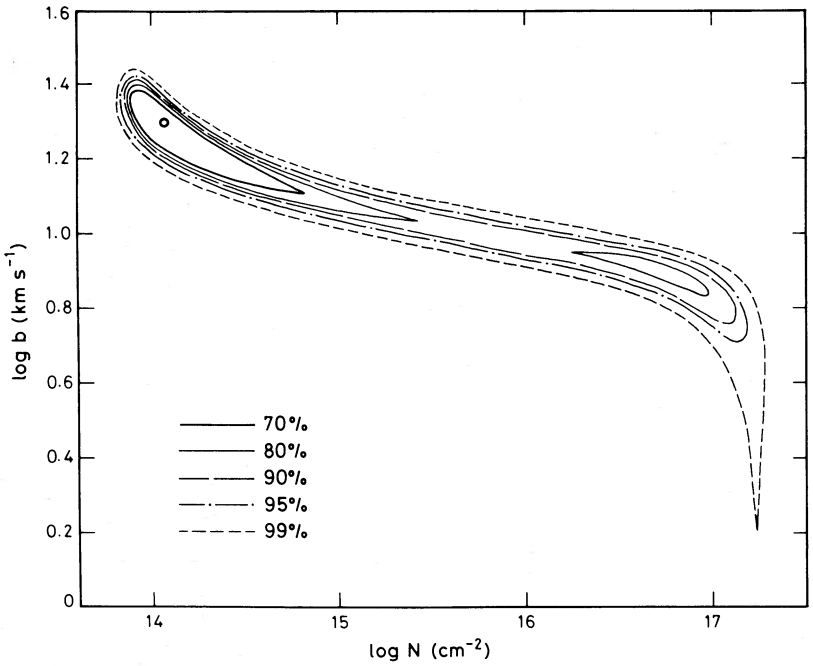


FIG. 2.—Confidence limits in the (log *b*, log *N*)-plane for a profile match to the observed Ly$\alpha$ line at $z_{abs} = 1.96358$

TABLE 2

ABSORPTION LINES

| n | $\lambda_{air}$ | $\lambda_{vac}$ | EW(A) | ± | ID | z | ± | b (km/s) | range | logN (/cm$^2$) | range[a] | Comments |
|---|---|---|---|---|---|---|---|---|---|---|---|---|
| A.1 | 3509.97 | 3510.97 | 0.99 | 0.06 | Lyα | 1.88814 | 0.00005 | 42 | 30–45 | 14.10 | 14.05–14.25 | |
| 2 | 3515.03 | 3516.03 | 1.86 | 0.05 | | 1.89193 | 0.00005 | 25 | 23–28 | 15.00 | 14.50–15.30 | |
| 3 | 3516.89 | 3517.89 | 0.77 | 0.04 | Lyα | 1.89278 | 0.00006 | 38 | 24–52 | 14.40 | 14.25–15.15 | |
| 4 | 3518.64 | 3519.64 | 1.19 | 0.04 | | 1.89389 | 0.00007 | 43 | 34–57 | 13.80 | 13.70–13.90 | |
| 5 | 3519.90 | 3520.90 | 0.80 | 0.04 | | 1.89522 | 0.00004 | 38 | 26–48 | 14.55 | 14.30–15.45 | |
| | | | | | | 1.89623 | 0.00003 | 36 | 28–43 | 14.15 | 14.05–14.35 | |
| 6 | 3525.05 | 3526.06 | 0.10 | 0.03 | Lyα | 1.90056 | 0.00011 | 14 | <36 | 13.05 | >12.75 | |
| 7 | 3526.35 | 3527.36 | 0.11 | 0.03 | Lyα | 1.90145 | 0.00010 | 2 | <28 | 13.50 | >12.30 | For b=10 km/s, logN=12.8 |
| | | | | | NV 1242 | 1.83835 | *b* | 10 | *b* | 13.80 | 13.50–14.00 | Possible identification |
| 8 | 3532.70 | 3533.71 | 0.15 | 0.03 | FeII 2600 | 0.35904 | 0.00002 | 3 | <15 | 14.35 | >12.90 | |
| 9 | 3533.23 | 3534.24 | 0.13 | 0.03 | FeII 2600 | 0.35922 | 0.00004 | 2 | <26 | 14.60 | >12.40 | |
| 10 | 3534.59 | 3535.60 | 0.11 | 0.02 | Lyα | 1.90839 | 0.00007 | 2 | <19 | 13.20 | >12.30 | For b=10 km/s, logN=12.8 |
| 11 | 3540.40 | 3541.41 | 0.19 | 0.03 | Lyα | 1.91315 | 0.00010 | 20 | 6–36 | 13.15 | 12.85–13.30 | |
| 12 | 3542.95 | 3543.96 | 1.29 | 0.05 | Lyα | 1.91454 | 0.00013 | 11 | <31 | 13.00 | >12.50 | |
| | | | | | | 1.91531 | 0.00004 | 40 | 34–47 | 14.25 | 14.15–14.40 | |
| 13 | 3546.82 | 3547.83 | 0.92 | 0.06 | Lyα | 1.91793 | 0.00020 | 30 | 12–100 | 13.05 | 12.75–13.40 | Alternatively, b<6.5 km/s, |
| | | | | | | 1.91847 | 0.00004 | 21 | 13–28 | 14.00 | 13.80–14.45 | logN=17.40 ± 0.15 (see text). |
| | | | | | | 1.91892 | 0.00005 | 2 | <22 | 16.00 | >13.05 | For b=10 km/s, logN=13.3 |
| 14 | 3557.10 | 3558.12 | 0.25 | 0.04 | Lyα | 1.92693 | 0.00017 | 35 | 20–72 | 13.20 | 12.95–13.40 | |
| 15 | 3559.75 | 3560.77 | 0.26 | 0.04 | Lyα | 1.92906 | 0.00007 | 24 | 16–34 | 13.40 | 13.25–13.50 | |
| 16 | 3570.27 | 3571.29 | 0.13 | 0.04 | Lyα | 1.93789 | 0.00014 | 13 | <60 | 12.80 | >12.35 | |
| 17 | 3575.79 | 3576.81 | 0.14 | 0.03 | | 1.83784 | 0.00005 | 7 | <18 | 12.80 | >12.50 | |
| 18 | 3577.17 | 3578.19 | 1.27 | 0.05 | SiII 1260 | 1.83835 | *b* | 6 | <20 | 12.80 | >12.50 | |
| | | | | | | 1.83870 | *b* | 15 | 12–19 | 13.85 | 13.70–13.95 | |
| | | | | | | 1.83905 | *b* | 9 | 6–11 | 13.80 | 13.70–13.95 | |
| | | | | | | 1.83938 | *b* | 20 | 15–33 | 13.20 | 13.05–13.30 | |
| 19 | 3578.79 | 3579.81 | 0.15 | 0.04 | Lyα | 1.94479 | 0.00009 | 25 | 13–41 | 13.20 | 13.00–13.35 | |
| 20 | 3580.87 | 3581.89 | 0.40 | 0.03 | Lyα | 1.94646 | 0.00003 | 19 | 14–25 | 13.70 | 13.60–13.85 | |
| 21 | 3588.77 | 3589.79 | 0.11 | 0.04 | Lyα | 1.95300 | 0.00017 | 18 | <52 | 12.90 | 12.45–13.10 | |
| 22 | 3598.72 | 3599.75 | 0.30 | 0.04 | Lyα | 1.96120 | 0.00005 | 17 | 11–26 | 13.40 | 13.25–13.50 | |
| 23 | 3601.72 | 3602.75 | 0.57 | 0.04 | Lyα | 1.96358 | 0.00003 | 19 | 13–24 | 14.10 | 13.85–14.80 | |
| 24 | 3613.98 | 3615.01 | 1.52 | 0.04 | Lyα | 1.97370 | 0.00002 | 35 | 25–40 | 14.95 | 14.65–16.20 | |
| 25 | 3616.95 | 3617.98 | 1.63 | 0.06 | Lyα | 1.97576 | 0.00010 | 55 | 43–73 | 13.70 | 13.60–13.80 | |
| | | | | | | 1.97677 | 0.00009 | 36 | 26–51 | 13.45 | 13.30–13.55 | |
| B.1 | 3695.68 | 3696.73 | 0.72 | 0.03 | OI 1302 | 1.83870 | *b* | 15 | *b* | 14.20 | 14.05–14.30 | |
| | | | | | | 1.83905 | *b* | 15 | 11–22 | 14.30 | 14.20–14.40 | |
| | | | | | | 1.83938 | *b* | 11 | *b* | 14.00 | 13.85–14.15 | |
| 2 | 3698.98 | 3700.03 | 0.90 | 0.04 | Lyα | 2.04361 | 0.00004 | 44 | 39–49 | 13.95 | 13.90–14.00 | |
| 3 | 3701.26 | 3702.31 | 0.96 | 0.03 | Lyα | 2.04540 | 0.00002 | 23 | 19–27 | 13.95 | 13.90–14.10 | |
| 4 | 3702.16 | 3703.21 | 0.39 | 0.03 | SiII 1304 | *b* | | *b* | | *b* | | |
| 5 | 3702.73 | 3703.78 | | | Lyα | 2.04672 | 0.00006 | 17 | 9–25 | 13.05 | 12.90–13.20 | |
| 6 | 3706.10 | 3707.15 | 0.63 | 0.03 | Lyα | 2.04944 | 0.00003 | 25 | 22–29 | 13.80 | 13.70–13.85 | |
| 7 | 3716.13 | 3717.19 | 0.20 | 0.03 | Lyα | 2.05774 | 0.00005 | 21 | 13–31 | 13.15 | 13.05–13.25 | |
| 8 | 3727.13 | 3728.19 | 0.24 | 0.03 | Lyα | 2.06681 | 0.00005 | 20 | 14–29 | 13.35 | 13.25–13.45 | |
| 9 | 3728.03 | 3729.09 | 0.40 | 0.03 | Lyα | 2.06752 | 0.00004 | 28 | 23–35 | 13.50 | 13.45–13.60 | |
| 10 | 3731.82 | 3732.88 | 0.18 | 0.03 | Lyα | 2.07061 | 0.00007 | 20 | 10–31 | 13.05 | 12.90–13.20 | |
| 11 | 3736.59 | 3737.65 | 0.35 | 0.02 | Lyα | 2.07465 | 0.00005 | 31 | 25–40 | 13.55 | 13.45–13.60 | |
| 12 | 3737.23 | 3738.30 | 0.23 | 0.02 | Lyα | 2.07513 | 0.00004 | 11 | <19 | 13.20 | >13.05 | |
| 13 | 3738.00 | 3739.07 | 0.53 | 0.02 | Lyα | 2.07572 | 0.00002 | 21 | 18–25 | 13.75 | 13.70–13.80 | |
| 14 | 3740.10 | 3741.17 | 0.84 | 0.03 | Lyα | 2.07741 | 0.00002 | 26 | 23–29 | 14.05 | 13.95–14.10 | |
| 15 | 3741.08 | 3742.15 | 0.30 | 0.02 | Lyα | 2.07822 | 0.00006 | 44 | 36–58 | 13.60 | 13.55–13.70 | |
| 16 | 3741.85 | 3742.92 | 0.36 | 0.03 | Lyα | 2.07892 | 0.00005 | 25 | 18–33 | 13.40 | 13.30–13.50 | |

TABLE 2—*Continued*

| n | $\lambda_{air}$ | $\lambda_{vac}$ | EW(A) | ± | ID | z | ± | b (km/s) | range | logN (/cm$^2$) | range[a] | Comments |
|---|---|---|---|---|---|---|---|---|---|---|---|---|
| 17 | 3746.39 | 3747.46 | 1.55 | 0.04 | Lyα | 2.08193 | 0.00005 | 18 | 12–26 | 13.20 | 13.05–13.30 | |
| | | | | | | 2.08272 | 0.00005 | 39 | 35–43 | 14.30 | 14.25–14.40 | |
| 18 | 3750.55 | 3751.62 | 0.20 | 0.03 | Lyα | 2.08602 | 0.00007 | 22 | 15–33 | 13.05 | 12.90–13.15 | |
| 19 | 3751.01 | 3752.08 | 0.11 | 0.02 | Lyα | 2.08679 | 0.00009 | 23 | 13–42 | 12.95 | 12.75–13.10 | |
| 20 | 3752.68 | 3753.75 | 0.82 | 0.03 | Lyα | 2.08780 | 0.00003 | 37 | 34–41 | 13.86 | 13.83–13.90 | |
| 21 | 3758.71 | 3759.78 | 0.16 | 0.02 | Lyα | 2.09282 | 0.00006 | 21 | 12–33 | 13.05 | 12.90–13.15 | |
| 22 | 3762.79 | 3763.86 | 0.10 | 0.03 | Lyα | 2.09614 | 0.00013 | 34 | 18–60 | 12.95 | 12.75–13.10 | |
| 23 | 3772.23 | 3773.30 | 1.20 | 0.03 | Lyα | 2.10390 | 0.00002 | 34 | 31–37 | 14.21 | 14.18–14.28 | |
| 24 | 3774.02 | 3775.09 | 0.13 | 0.02 | Lyα | 2.10531 | 0.00010 | 30 | 19–47 | 12.95 | 12.80–13.10 | |
| 25 | 3786.16 | 3787.23 | 0.12 | 0.02 | CII 1334 | 1.83786 | 0.00004 | 11 | <19 | 13.40 | >13.25 | |
| 26 | 3787.43 | 3788.50 | 1.01 | 0.02 | | 1.83835 | 0.00002 | 7 | <13 | 13.55 | >13.40 | |
| 27 | 3788.33 | 3789.40 | 0.22 | 0.02 | | 1.83870 | *b* | 11 | 9–14 | 14.40 | 14.30–14.85 | |
| | | | | | | 1.83905 | *b* | 14 | 12–16 | 14.40 | 14.30–14.60 | |
| | | | | | | 1.83938 | 0.00003 | 11 | <16 | 13.70 | >13.60 | |
| 28 | 3791.69 | 3792.76 | 0.30 | 0.02 | MgII 2796 | 0.35635 | 0.00001 | 11 | – | 12.6 | – | $z_{abs}$=0.35631 |
| | | | | | | | | 5 | – | 12.8 | – | $z_{abs}$=0.35642 |
| 29 | 3795.37 | 3796.44 | 0.06 | 0.02 | Lyα | 2.12305 | 0.00030 | 53 | 35–90 | 13.00 | 12.85–13.15 | |
| 30 | 3799.28 | 3800.36 | 0.34 | 0.01 | MgII 2796 | 0.35903 | 0.00001 | 9 | 6–10 | 13.39 | 13.30–13.70 | |
| 31 | 3799.82 | 3800.90 | 0.33 | 0.01 | | 0.35923 | 0.00001 | 14 | 12–16 | 13.08 | 13.04–13.11 | |
| 32 | 3801.62 | 3802.70 | 0.26 | 0.02 | MgII 2803 | 0.35638 | 0.00001 | 11 | – | 12.6 | – | $z_{abs}$=0.35631 |
| | | | | | | | | 5 | – | 12.8 | – | $z_{abs}$=0.35642 |
| 33 | 3803.47 | 3804.55 | 0.60 | 0.02 | Lyα | 2.12955 | 0.00003 | 41 | 38–46 | 13.66 | 13.63–13.70 | |
| 34 | 3804.49 | 3805.57 | 0.19 | 0.02 | Lyα | 2.13033 | 0.00005 | 31 | 24–39 | 13.20 | 13.10–13.25 | |
| 35 | 3809.02 | 3810.10 | 0.29 | 0.01 | MgII 2803 | 0.35904 | 0.00001 | 9 | 6–10 | 13.39 | 13.30–13.70 | |
| 36 | 3809.57 | 3810.65 | 0.26 | 0.01 | | 0.35922 | 0.00001 | 13 | 12–16 | 13.08 | 13.04–13.11 | |
| C.1 | 4332.69 | 4333.90 | 0.19 | 0.03 | SiII 1526 | 1.83870 | 0.00003 | 15 | 12–19 | 13.85 | 13.70–13.95 | |
| 2 | 4333.22 | 4334.44 | 0.19 | 0.03 | | 1.83905 | 0.00004 | 9 | 6–11 | 13.80 | 13.70–13.95 | |
| 3 | 4392.25 | 4393.48 | 0.29 | 0.03 | CIV 1548 | 1.83786 | *b* | 24 | 17–29 | 13.55 | 13.45–13.65 | |
| 4 | 4392.95 | 4394.19 | 0.29 | 0.02 | | 1.83835 | *b* | 18 | 13–23 | 13.55 | 13.45–13.60 | |
| 5 | 4393.55 | 4394.78 | 0.28 | 0.02 | | 1.83870 | *b* | 14 | 8–18 | 13.50 | 13.35–13.55 | |
| 6 | 4394.31 | 4395.54 | 0.42 | 0.02 | | 1.83913 | 0.00002 | 15 | 11–18 | 13.77 | 13.70–13.81 | |
| 7 | 4399.59 | 4400.82 | 0.14 | 0.02 | CIV 1550 | 1.83786 | *b* | 25 | 17–29 | 13.55 | 13.45–13.65 | |
| 8 | 4400.59 | 4401.82 | 0.36 | 0.03 | | 1.83835 | *b* | 18 | 13–23 | 13.55 | 13.45–13.60 | |
| 9 | 4401.62 | 4402.85 | 0.28 | 0.02 | | 1.83870 | *b* | 14 | 8–18 | 13.50 | 13.35–13.55 | |
| | | | | | | 1.83913 | 0.00003 | 15 | 11–18 | 13.77 | 13.70–13.81 | |

[a] Where no upper limit is given, that derived using an arbitrary minimum value of *b* of 1 km s$^{-1}$ is about 15.0–16.0.

[b] Parameters set by other lines in the system.

NOTE.—The wavelengths have been corrected to heliocentric values. Vertical bars indicate blended features. Continuum fitting errors have not been included in estimating the errors in the equivalent widths of the lines, but trials with different continuum estimates suggest that the additional uncertainty from this is usually about 0.02 Å.

$f = 0.0764$, and Shull, Snow, and York (1981), from observational evidence, suggest $f = 0.23$ is more appropriate. In contrast with Shull, Snow, and York, we cannot obtain a consistent solution with Si II $\lambda$1260 $f = 0.959$ and Si II $\lambda$1526 $f = 0.23$. With these oscillator strengths, if we take the values predicted from the $\lambda$1260 line alone (which are close to those given in Table 3), then the predicted $\lambda$1526 lines are at least twice as deep as those observed. This problem is eased completely by adopting $f = 0.0764$ for $\lambda$1526, though at $z_{abs} = 1.83905$ the predicted Si II $\lambda$1304 line then appears to be a little too strong. In compiling Tables 2 and 3 we have therefore adopted Si II $\lambda$1526 $f = 0.0764$ and, because it is blended, ignored the Si II $\lambda$1304 line except as a consistency check. Our results are in agreement with the recent theoretical values of the oscillator strengths published by Dufton *et al.* (1982).

There is, however, another possibility, and that is that a Lyα feature is blended with Si II $\lambda$1260. This would cause us to overestimate the Si II column density based on this line alone. While we cannot rule this out, the good redshift agreement between the components of the Si II $\lambda$1260 and other lines in the complex (notably C IV $\lambda\lambda$1548, 1550) suggests that an additional sharp Lyα is not present there in any significant strength.

The Fe II $\lambda$1260 line is sufficiently far from Si II $\lambda$1260 that the two should be just resolved in our data. There is possible contamination of some Si II $\lambda$1260 lines by Fe II from a

TABLE 3

COLUMN DENSITIES IN $z_{abs} = 1.8387$ COMPLEX

| Ion | $b$* | $z = 1.83785$ | | $z = 1.83835$ | | $z = 1.83870$ | | $z = 1.83905$ | | $z = 1.83938$ | |
|---|---|---|---|---|---|---|---|---|---|---|---|
| | | 10 | | 10 | | 15 | | 10 | | 11 | |
| | | $b$ | log $N$ | $b$ | log $N$ | $b$ | log $N$ | $b$ | log $N$ | $b$ | log $N$ |
| C I | | | < 12.95 | | < 12.70 | | < 13.20 | | < 13.10 | | < 12.80 |
| C II | | 11 | 13.40 | 7 | 13.55 | 15 | 14.40 | 11 | 14.40 | 11 | 13.70 |
| C II* | | | < 12.80 | | < 12.85 | | < 12.95 | | < 13.15 | | bl |
| C IV | | 24 | 13.55 | 18 | 13.55 | 14 | 13.50 | 15 | 13.80[a] | | < 12.75 |
| N V | | | < 13.35 | | 13.80[b] | | < 13.40 | | < 13.60 | | < 13.35 |
| O I | | | < 13.60 | | < 13.65 | (15) | 14.20 | 15 | 14.30 | (11) | 14.00 |
| O I* | | | bl | | bl | | bl | | < 13.40 | | < 13.35 |
| O I** | | | < 13.60 | | bl | | bl | | < 13.60 | | < 13.50 |
| Si II | | 7 | 12.80 | 6 | 12.80 | 15 | 13.85 | 9 | 13.80 | 20 | 13.20 |
| Si II* | | | < 12.60 | | < 12.80 | | < 12.65 | | < 12.60 | | < 12.60 |
| Si II | | | < 14.20 | | < 13.95 | | < 14.00 | | < 14.25 | | < 14.05 |
| Fe II | | | < 14.60 | | bl | | bl | | bl | | bl |
| Electron density ($cm^{-3}$) | | | < 10 | | < 8 | | < 1.4 | | < 2.1 | | |

[a] Preferred redshift $z = 1.83913$.

[b] Line blended, identification may be incorrect.

NOTE.—$b$* is the value of the $b$-parameter (in km $s^{-1}$) used in obtaining column density upper limits. bl, component blended with another line. Velocity dispersions in parentheses were arbitrarily chosen values, consistent with the data.

lower redshift component within the complex, but trials with an assumed Fe II/Si II abundance ratio of unity showed that the Fe II oscillator strength is sufficiently low that its contribution may safely be ignored.

A further detailed point is that since the data were rebinned to a uniform wavelength scale, the counting error is not independent from channel to channel, though the channel size is approximately the same as in the raw data so that only neighboring channels are correlated. Since there is nearly the same number of data points in any line profile as in the original spectrum, it is unlikely that our error estimates are very far from reality. (Some rebinning of the data is necessary because small system drifts over long exposure time have to be corrected for if the highest possible resolution is to be attained. The use of a uniform wavelength scale is merely for convenience).

Checks were made by estimating parameters for each component separately in relatively clean Mg II and C IV doublets, and then intercomparing these for internal consistency. The strong C IV components at $z_{abs} = 1.83913$ (§ III) and the Mg II doublets at $z_{abs} = 0.35903$ (§ IV) gave excellent agreement. The Mg II doublet at $z_{abs} = 0.35635$ (§ IV) yielded rather disparate column densities, though the velocity dispersion estimates agree well. We suspect that this discrepancy arises because unresolved velocity structure is present in this case. The other examples suggest that single clouds with Gaussian velocity dispersions dominate these lines, and also serve to confirm that the method of analysis we have adopted is sound.

## III. THE $z_{abs} = 1.8387$ COMPLEX

The $z_{abs} = 1.8387$ system found at lower resolution by Carswell *et al.* (1982) shows complex component structure, as is clearly seen in Figure 1 and from Table 2. Five components to the system are evident in our data, and there appear to be discrepancies in velocity dispersion estimates (but usually not redshifts) between lines of different stages of ionization, so there may be further undetected structure. The heliocentric redshifts, and details of the five components we have found, are given below:

$z_{abs} = 1.83785$. The redshift was determined from the C II $\lambda$1334 and Si II $\lambda$1260 lines, with both C II and Si II yielding a velocity dispersion $b = 10$ km $s^{-1}$, with an upper limit of $\sim$20 km $s^{-1}$. For C IV $\lambda\lambda$1548, 1550 the line blending is more severe, so the velocity dispersion and column densities were determined using the adopted redshift of $z_{abs} = 1.83785$. Then the best estimates for the C IV doublet lines independently yielded $b$-parameters of close to 25 km $s^{-1}$, but the errors are also rather large. Choosing 10 km $s^{-1}$ gave a worse, but still acceptable, fit to the short wavelength wings of the C IV blends.

For any other ions which may give absorption lines in the observed wavelength range, notably O I, no significant features were found at this redshift. Table 3 gives 95% confidence upper limits for these, obtained using a velocity dispersion $b^* = 10$ km $s^{-1}$ and using the profile fitting technique described in § II.

$z_{abs} = 1.83835$. This is a component which is required to explain structure in C II $\lambda$1334, Si II $\lambda$1260, and C IV $\lambda\lambda$1548, 1550. The redshift is the least well defined in the complex, but the value given here is at worst internally consistent with the others. The most notable feature about this system is the tentative identification of N V $\lambda$1242 at a redshift consistent with this, though a blend with Ly$\alpha$ at $z_{abs} = 1.90145$ is required to explain the whole of the feature at $\lambda_{vac} = 3527.36$. If the whole feature is identified as N V $\lambda$1242, the redshift is discrepant. The corresponding N V $\lambda$1238 line falls in the strong complex feature at 3516 Å, and so it is completely undetectable. The velocity dispersion for C IV $\lambda\lambda$1548, 1550 is higher than found for C II $\lambda$1334 and Si II $\lambda$1260, but the difference is not significant.

$z_{abs} = 1.83870$. The redshift is defined by the only line which is not badly blended, Si II $\lambda$1526. Ionization stages from O I to C IV are present.

$z_{abs} = 1.83905$. The strong features in the C IV complexes give a redshift of $z_{abs} = 1.83913$, and an independent lower determination of 1.83905 comes from Si II $\lambda$1526. It is possible that there are two systems, one high ionization and one low, but the errors in redshift indicate that the data are just compatible with a single cloud. We have kept them separate here, preferring the $z_{abs} = 1.83905$ value for all but the C IV lines. Any differences in $b$-parameters and column densities derived using these instead of a mean redshift are small.

$z_{abs} = 1.83938$. This redshift is shared by C II $\lambda$1334, Si II $\lambda$1260, and O I $\lambda$1302 in our spectra, with the C II line being relatively clear, so it was used to set the redshift. C IV $\lambda\lambda$1548, 1550 were not detected.

With those components, the derived physical parameters of which are summarized in Table 3, each observed line profile in the $z_{abs} = 1.8387$ complex is well reproduced. The match to the C IV $\lambda\lambda$1548, 1550 doublet is shown in Figure 3. However, the results may well depend on the decomposition into components chosen. Nonetheless it is encouraging that the two lines of the C IV doublet give consistent results and the velocity components generally agree from ion to ion. The total column densities of Si II and C IV over the whole complex are $10^{14.2}$ cm$^{-2}$ in both cases, in remarkably good agreement with $10^{14.6}$ and $10^{14.1}$, respectively, from the lower resolution estimates by Carswell *et al.* (1982).

The most uncertain values are those determined for C II at redshifts $z_{abs} = 1.83870$ and 1.83905. The lines are optically thick, and the profile match depends critically on the strengths of the weaker components on either side of these two. Also, we do not have a second C II line to help give us an independent estimate of the velocity dispersions and column densities. The same remarks apply to O I, particularly for $z_{abs} = 1.83905$.

Table 3 also contains limits to the electron density in each component determined from the nondetection of the C II* $\lambda$1335.7 fine structure line. We have chosen a temperature of $10^4$ K in the calculations, and used the expression derived by Bahcall and Wolf (1968).

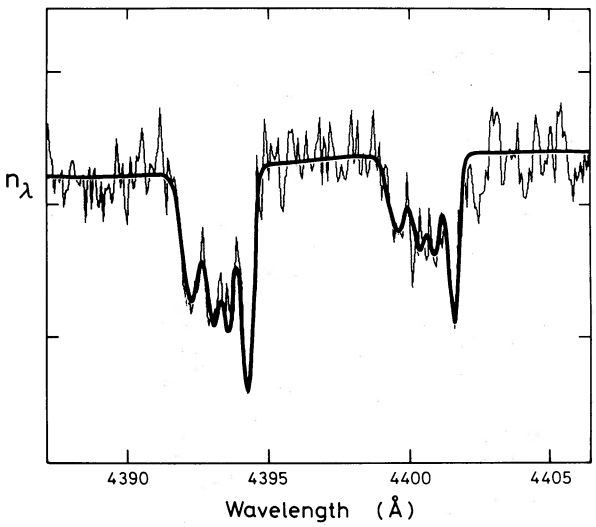


FIG. 3.—The complex C IV lines at $z_{abs} = 1.8387$, with the best fit (solid line) superposed.

The velocity spread over the line complex is 160 km s$^{-1}$, which does not exclude the possibility that we are looking through a galaxy or galaxy halo, though the number of clouds seen is higher than we might normally expect (see York 1982) and the velocity spread may also be larger (see Weisheit and Collins 1976). Unfortunately, we have obtained spectroscopic data for the lines of only a few ions, so it is difficult to compare our results with those obtained for the high ionization species in the halo of our Galaxy (Savage and de Boer 1979; Pettini and West 1982) and the Magellanic Clouds (de Boer and Savage 1980). However, we do find that N V is weak compared with C IV, as is usual for our galactic halo and QSO absorption systems generally. The low ionization lines (C II, O I, and Si II) are weaker relative to C IV than is shown by the Galactic and Magellanic Cloud observations, but it is not clear that most of the low ionization absorption necessarily occurs in the haloes.

Pettini and West (1982) draw attention to the $N$(C IV)/$N$(Si IV) ratio as a possible discriminator between disk and halo gas. For observations in the Galactic plane they find this ratio is $0.60 \pm 0.5$, and the halo gas gives $4.5 \pm 1.5$. We do not have high-resolution spectra of the Si IV $\lambda\lambda$1393, 1402 doublet, but Carswell *et al.* (1982), from low-resolution material, find $N$(Si IV) = $10^{14.1}$ cm$^{-2}$. Unfortunately, combining this with the $N$(C IV) = $10^{14.2}$ cm$^{-2}$ found earlier gives $N$(C IV)/$N$(Si IV) = 1.25, which is inconclusive.

If the absorption complex arises in the outer regions of an intervening rotating galaxy or halo, and the absorbing clouds share the galaxy rotation, then we might expect the ionization to be a function of the cloud redshift within the complex. Unless the galaxy is face-on, the cloud speed projected along any line of sight will have a maximum amplitude relative to the galaxy rest system nearest the galaxy center, and fall off at least as fast as a cosine law along the light path. If there is any correlation of ionization with distance (through, e.g., a density falloff), then it will show up as an observed ionization-velocity correlation in the component clouds if they are resolvable (see Weisheit and Collins 1976 for model calculations). This appears to be the case for the $z_{abs} = 1.8387$ complex, where the ionization, as measured by the C IV/C II ratio, probably decreases with increasing redshift, as is shown in Figure 4.

Note also that the suggested ionization-velocity correlation is not consistent with that expected if the absorbing complex is ejected from the QSO. It is difficult to understand how the velocities can be close together if the distance from the quasar does not increase with the velocity relative to the quasar, so the highest redshift cloud must then be the one subjected to most of the ionizing radiation and, if the densities of all are comparable, be the most highly ionized. At least some of the clouds are optically thick to Lyman continuum radiation (Boksenberg and Snijders 1981), so shielding by other clouds in the complex would give the result that the ionization should increase with increasing redshift. If there is any trend, it is the opposite.

It is also instructive to compare the derived column densities with predictions based on a simple model. This will be of limited value since we have measured quantities for only four ions—C II, C IV, O I, and Si II. We suppose that the dominant

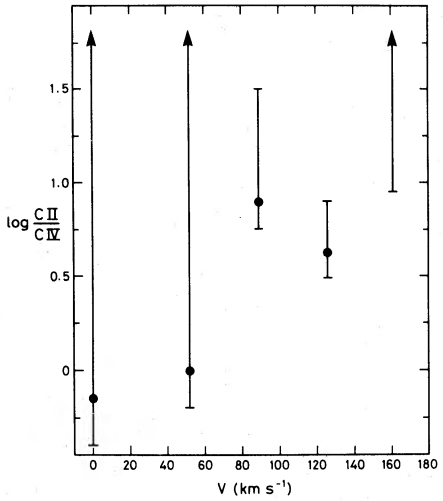


FIG. 4.—The C II/C IV number ratio for components of the $z_{abs} = 1.8387$ complex.

ionization mechanism is the integrated background QSO light (cf. Arons and Wingert 1972; Röser 1975; Sargent *et al.* 1979). For a power law spectral index $\alpha = 0.75$, the radiation intensity at 1 rydberg is $7.6 \times 10^{-22}$ ergs cm$^{-2}$ s$^{-1}$ Hz$^{-1}$ sr$^{-1}$ at redshift $z = 1.84$ (see Sargent *et al.* for the assumptions made, and details of the derivation of this quantity). We assume the clouds have constant density, solar abundances, and a simple slab geometry with the light path perpendicular to the slab.

Table 4 contains the results of such a calculation, where the cloud ionizations and optical depths were determined by matching to the observed C II and C IV column densities. Thus the predicted quantities which may be compared with those derived from the observations are the O I and Si II column densities. The observed Si II column densities are a factor of 2 or 3 higher than predicted, which is fair agreement given the uncertainties, but the observed O I values are high by factors of over 10 in the three highest redshift components where the O I line was detected. Also the predicted total H I column density in the model is only $10^{17}$ cm$^{-2}$, which is lower by a factor of 5 than required by the Lyman limit observations described by Boksenberg and Snijders (1981).

Obviously the discrepancies are removed to some extent if the heavy element abundance is considerably below the solar value, since then the Lyman continuum optical depth will be higher and the C II and C IV lines arise predominantly in separate zones of each cloud. However, even abundances $\sim 1/10$ solar do not make the O I descrepancy much better. But before seeking astrophysical reasons for the differences, it is worth considering the limitations imposed by the data. The most obvious points are that we do not know if any of the O I, C II, or Si II $\lambda$1260 lines are blended with Ly$\alpha$ at another redshift, and that the individual component column densities are not well determined because of the presence of the other nearby redshift systems. Additionally, the cloud parameters have been derived assuming that both low and high ionization lines arise predominantly in the same regions. There are indications that this might not be the case, particularly at $z_{abs} = 1.83905$, where the Si II $\lambda$1526 and C IV $\lambda\lambda$1548, 1550 redshifts are only just consistent. At other redshifts the differences in the velocity dispersion estimates are also suggestive of further component structure.

## IV. OTHER REDSHIFT SYSTEMS

### *a) The $z_{abs} = 0.3591$ Complex*

Interestingly, the strong lines just shortward of the peak of the Ly$\alpha$ emission line shown in Figure 5 are identified not with the Ly$\alpha$ but with a complex Mg II system, with redshifts 0.35903 and 0.35923 and so a velocity separation of 40 km s$^{-1}$. Confirmation comes from identification of Fe II $\lambda$2600 at these redshifts. A second Fe II feature, at $\lambda$2586, should fall in the strong Ly$\alpha$ complex at 3515–3520 Å, and so is not measurable. Fe II/Mg II in the two clouds are 1.05 and 0.66, respectively, for the velocity dispersion parameters shown in Table 2, but the uncertainties in Fe II in particular are large and so this difference is not significant.

There is probably a third, weaker system visible only in Mg II at $z_{abs} = 0.35635$ which is 590 km s$^{-1}$ from $z_{abs} = 0.35904$. We cannot exclude the possibility of two Ly$\alpha$ lines at just the right separation, but this is not very likely. The lines appear to be resolved, but no component structure is discernible. This third doublet is not at all well fitted by a single cloud with Gaussian velocity dispersion, so there is unresolved velocity structure present. We have not explored the region of acceptable parameters very far, but it is possible to reproduce the profiles with two clouds at redshifts 0.35631 and 0.35642, Mg II column densities $4 \times 10^{12}$ and $6 \times 10^{12}$ cm$^{-2}$, and velocity parameters of 11 and 5 km s$^{-1}$, respectively. Thus the

TABLE 4

MODEL CLOUD PARAMETERS

| PARAMETER | $z_{abs}$ 1.83785 | 1.83835 | 1.83870 | 1.83905 | 1.83838 |
|---|---|---|---|---|---|
| $\Delta v$ (km s$^{-1}$) | 0 | 53 | 90 | 127 | 162 |
| log $n$(H) | −1.25 | −1.20 | −0.90 | −1.00 | > −0.88 |
| log $N$(H I) | 15.60 | 15.75 | 16.65 | 16.60 | 15.90[a] |
| log $N$(C II) | 13.40 | 13.55 | 14.40 | 14.40 | 13.70 |
| log $N$(C IV) | 13.55 | 13.55 | 13.50 | 13.80 | < 12.75 |
| log $N$(O I) | 11.55 | 11.75 | 13.10 | 12.95 | 12.40[a] |
| log $N$(Si II) | 12.30 | 12.50 | 13.65 | 13.60 | 12.95[a] |

[a] Values calculated assuming log $N$(C IV) = 12.75. For smaller values of $N$(C IV), the H I and O I column densities are larger.

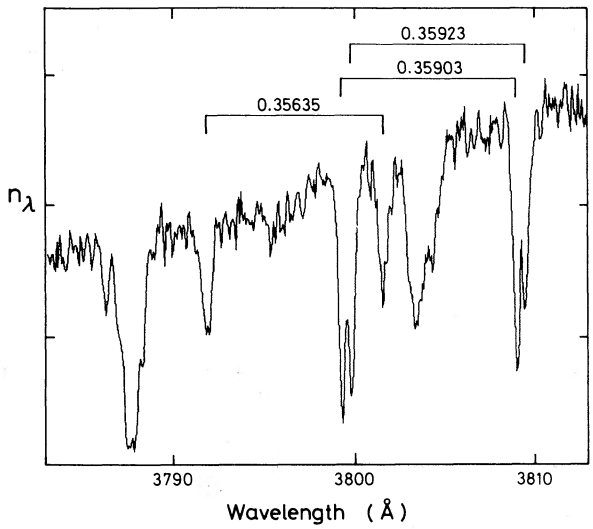


FIG. 5.—The Mg II absorption doublets in the wing of the Lyα emission line with redshifts marked. The feature at 3787.5 Å is due to C II λ1334 in the $z_{abs} = 1.8387$ complex.

velocity separation between these two components is of order 24 km s$^{-1}$. The total velocity spread over the whole low-redshift complex is 630 km s$^{-1}$, which is somewhat large to be due to a single galaxy, but is about that expected from a cluster. It is therefore quite likely that the light we see from Q1101−264 is passing through two galaxies in a cluster, each with two clouds along the line of sight.

A number of faint galaxies are discernible on a CTIO 4 m IIIa-J plate obtained for us by Dr. John Graham. We have attempted to determine redshifts for those galaxies marked in Figure 6 (Plate 4), using the Cassegrain spectrographs at the Anglo-Australian 3.9 m, Mauna Kea 2.2 m, and Cerro Tololo 4 m telescopes. Our results are summarized in Table 5. Of the three redshifts we have determined so far, two are considerably lower than that of any component of the absorption complex, and one, at $z = 0.370$ from two independent spectra, is slightly (but significantly) higher than the highest absorption component $z_{abs} = 0.3592$. The velocity difference is 2400 km s$^{-1}$, which is rather large to be attributable to velocity dispersion in a normal cluster of galaxies, but the redshifts are sufficiently close that it is tempting to say the quasar absorption system and the galaxy may be associated in some way. It would clearly be of value to obtain redshifts for other galaxies in the field.

### b) *Comments on Other Systems*

A possible C IV λλ1548, 1550 doublet $z_{abs} = 1.4202$ from the two lines at 3747 and 3753 Å has been suggested by Young, Sargent, and Boksenberg (1982). The wavelength agreement for these lines is quite good, but the poor matching of profiles suggests that this system can be discounted.

Another tentative system near the emission redshift, based on the C IV doublet at $z_{abs} = 2.1250$, was suggested by Carswell *et al.* (1982). We see no sign of a corresponding Lyα line, so the reality of this system, and of the C IV absorption lines themselves, remains very doubtful. Wilkes (private communication) and Young, Sargent, and Boksenberg (1982) do not see these lines in their lower resolution (and poorer signal-to-noise) data. Note, though, that comparison of Carswell *et al*'s equivalent widths (which generally agree well with ours) with those of Young *et al.* shows that the latter systematically underestimate the equivalent widths of absorption lines which occur in emission features. If this is true in all their objects, it may provide a partial explanation for the absence of systems with $z_{abs} \sim z_{em}$ that they find in contrast with the Weymann *et al.* (1979) and Weymann, Carswell, and Smith (1981) results.

## V. THE Lyα LINES

The most striking feature of the Lyα lines in the two spectral regions is that almost all are resolved at our limiting *b*-parameter of ∼10 km s$^{-1}$. The velocity dispersion parameters tend to lie in the range 10–45 km s$^{-1}$, in general agreement with the results obtained for a few lines at higher redshifts by Chaffee *et al.* (1982, 1983). A few cases appear to be narrower, but these are the weakest lines where the values derived are the most suspect. Line blending, where it occurs, adds to the uncertainty in the results, but even in the clear single absorption lines the same general trend is evident (see Fig. 7), with the velocity dispersion parameter *b* concentrating in the range 15–25 km s$^{-1}$.

The H I column densities are, as expected, low, with most of the lines detected arising in material with $10^{13} < N(\text{H I}) < 10^{14}$ cm$^{-2}$. There is no reason why higher column densities should have been missed if they are present, since we attempted to find the minimum number of components to adequately represent any broad feature, but this may have introduced a bias against low velocity dispersion components in blended lines. Individual low column density clouds, with $N(\text{H I}) < 8 \times 10^{12}$ cm$^{-2}$, would not normally have been detected.

An equivalent width distribution function may be fitted to

TABLE 5

GALAXIES IN THE FIELD OF Q1101−264

| Object No. | Telescope | Exposure Time (min) | Redshift | Comments |
|---|---|---|---|---|
| 2 | AAT | 460 | ... | Inconclusive spectra |
| | Mauna Kea | 50 | | |
| 3 | AAT | 350 | 0.18: | H & K break |
| 6 | Mauna Kea | 100 | 0.297 | [O II], H & K |
| 7 | Mauna Kea | 50 | ... | Inconclusive spectra |
| | CTIO | 180 | | |
| 9 | Mauna Kea | 100 | 0.370 | H & K |
| | CTIO | 180 | | |

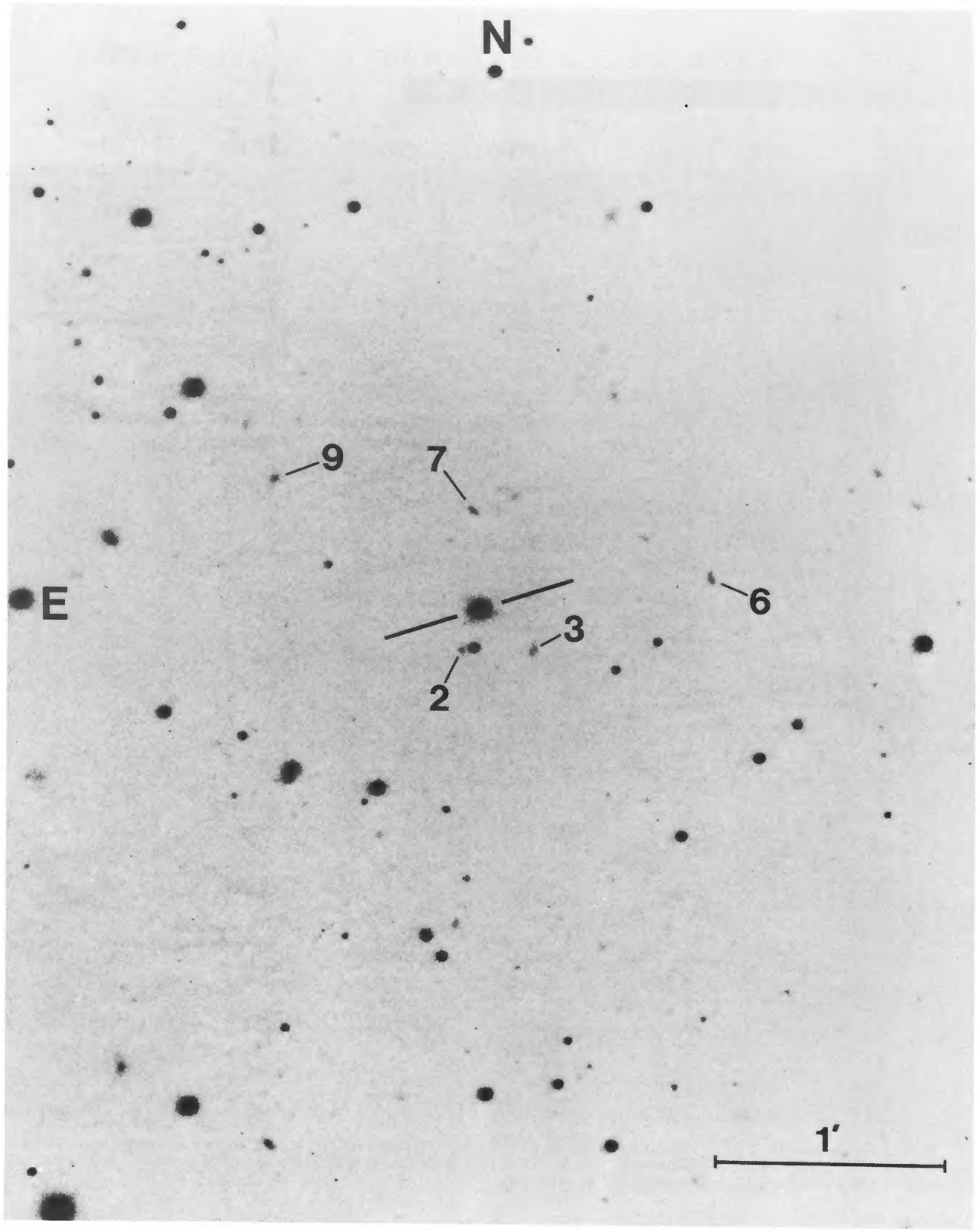


FIG. 6.—A CTIO 4 m IIIa-J plate of the Q1101−264 field. Numbers are shown against the candidate galaxies for which spectra were obtained.

CARSWELL *et al.* (*see* page 495)

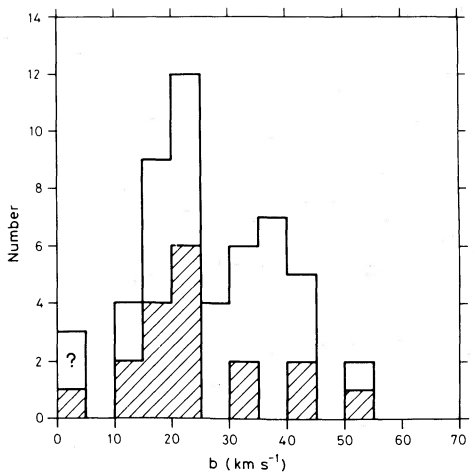


FIG. 7.—The H I velocity dispersion distribution for the Lyα lines. Lines which are entirely free from possible blending effects are shown shaded. The three cases with $b < 5$ km s$^{-1}$ were determined from weak lines and are uncertain (see Table 2).

the data presented in Table 2 using the Sargent *et al.* (1980) form,

$$p(W, z) = A/W^* \exp(-W/W^*)\, dWdz$$

for rest Lyα equivalent width $W$ and redshift $z$. The maximum likelihood values (see, e.g., Kendall and Stuart 1967) for $z = 2$ and $W > 0.033$ Å are:

$$A = 264 \pm 8\ (1\ \sigma)\,,$$
$$W^* = 0.16 \pm 0.02\,.$$

For the clear single Lyα lines $W^* = 0.07 \pm 0.02$ Å, the difference perhaps reflecting deficiencies in our line deblending criteria. The value of $W^*$ is not very sensitive to the detection limit equivalent width chosen. For example, if we restrict consideration to all lines with $W > 0.075$ Å, $W^* = 0.19 \pm 0.04$.

Note that Sargent *et al.* (1980) found, for a much larger but lower resolution sample, $A = 154 \pm 11$ and $W^* = 0.36 \pm 0.02$ Å. We believe that most of the difference between the derived parameters in these two investigations can be attributed to differences in the resolution. Undoubtedly we consider as multiple many lines which Sargent *et al.* would have regarded as being single features. Profile fitting also occasionally further divides the lines into components, though to be directly comparable with the earlier work we have not used these in the derivation of the equivalent width distribution function.

The column density distribution is poorly fitted by the form of exponential used for the equivalent widths, despite the fact that many of the lines are optically thin. For $N(\text{H I}) > 10^{13}$ cm$^{-2}$, we find that a power law of the form

$$p(N, z) = BN^{-s}dNdz$$

adequately fits the data, with $B = (s - 1)\,(10^{13})^{s-1} \times B_0$ with $s = 1.68 \pm 0.10$ and $B_0 = 225 \pm 34$. However, using a power law of this form also contains the implicit assumption that it is invalid at low column densities if the cloud numbers are to be finite; i.e., in the simplest form there must be a low density cutoff. The cutoff cannot be far below our detection limit, since the continuum regions of the spectrum show no signs of the population of weak lines predicted by extrapolating the $p(N, z)$ relation to $N(\text{H I}) = 10^{12}$ cm$^{-2}$. Numerical trials show that the number of lines for which $10^{12} < N(\text{H I}) < 10^{13}$ cm$^{-2}$ must be at least a factor of 2 or 3 lower than that predicted by the power law. Thus the choice of a power law is probably not a good one, but a better determination of the column density distribution function must await a more extensive study. Note that a very obvious simple model, that of spheres with equal column densities where the differences in path length through the cloud give rise to the range of observed values, does not fit the observed distribution. So, unsurprisingly, there must be an intrinsic distribution in the central H I optical depths in the clouds.

The problems introduced by line blending suggest that the two-point correlation function between the Lyα lines might show a peak at low velocity separations. There is a suggestion of such a peak for separations below about 400 km s$^{-1}$, but this peak is not statistically significant. So, from this small sample, there is no significant evidence for clustering of the clouds for velocities above a lower limit of 50 km s$^{-1}$. The absence of such a peak, if confirmed from a larger sample, would show that the clouds are not clustered on scales which would be appropriate for quite small galaxies or clusters, and reinforce the case for their being intergalactic.

There is somewhat marginal evidence for a correlation between velocity dispersion and H I column density, as might be expected if, for example, the clouds are partially confined by self-gravity as proposed by Melott (1980) and Black (1981). This apparent correlation arises from a dearth of systems with low velocity dispersion ($b < 20$ km s$^{-1}$) and high H I column density ($N > 3 \times 10^{13}$ cm$^{-2}$). It is not clear if blending of the higher column density systems contributes to this effect, and in any case more observational data are required before it can be estimated.

A number of model calculations have suggested that the Lyα absorbing clouds should have temperatures in the range $10^4$–$4 \times 10^4$ K (Sargent *et al.* 1980; Weymann, Carswell, and Smith 1981) to as high as $6 \times 10^4$–$9 \times 10^4$ K (Black 1981). Since we are able to measure velocity dispersions as low as $b = 13$ km s$^{-1}$ corresponding to temperatures of $10^4$ K in hydrogen, we are able to check these predictions. There are some cases where the upper limits to the velocity parameters indicate temperatures which *must* be as low as $2 \times 10^4$ K, and many appear to be in the range $10^4$–$4 \times 10^4$ K, or rather lower than the values suggested on Black's model. Note that the velocity dispersions we derive provide only an upper limit to the temperatures. We can not exclude the possibility that turbulence or bulk motions broaden the lines beyond their thermal widths; indeed, it is difficult to understand how the large velocity parameters (>40 km s$^{-1}$) can arise if this is not occurring in at least some cases. The fact that most of our temperatures, derived on the assumption that we are seeing the thermal widths, agree fairly well with some models may be fortuitous.

In principle we may estimate (or in practice obtain lower limits for) the densities in most of the clouds if we assume that the velocity dispersion measured is entirely due to thermal motion, and that the cloud heating is solely from the diffuse quasar background radiation (cf. Sargent *et al.* 1979). We have adopted the Sargent *et al.* values for the quasar background

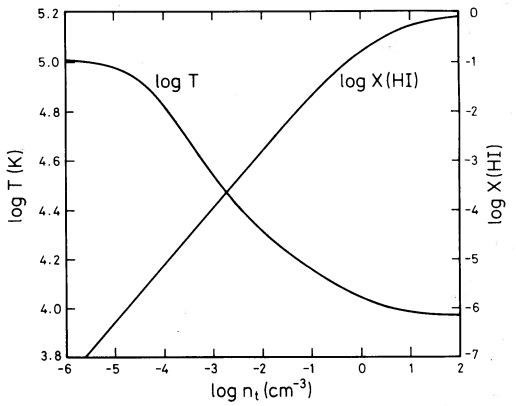


FIG. 8.—The temperature–total hydrogen density ($n_t = n_p + n_{\rm H\,I}$) dependence for optically thin clouds heated by background quasar radiation at $z = 2$. Also shown is the neutral hydrogen fraction $X$(H I).

corrected to redshift $z = 2$, assumed zero metal abundances, and used the rate equations given by Black (1981) to derive a temperature-density curve for the clouds (Fig. 8). The total range of possible temperatures on this model is about $10^4$–$10^5$ K, or velocity dispersions from 13 to 41 km s$^{-1}$, and some of our systems have values outside this range. While there are no cases where the velocity dispersion must be below the model limit, there are a number where it must, on the basis of the error range, be somewhat higher. We exclude all these values from the density determinations, but they serve as a reminder that we cannot always necessarily interpret Doppler velocities as temperatures. However, most of the velocity dispersions may be interpreted as acceptable temperatures on this model, and they generally give rise to total hydrogen density estimates in the approximate range $10^{-4}$ to $10^{-2}$ cm$^{-3}$, as suggested by Sargent *et al.* (1980) and Weymann, Carswell, and Smith (1981). The distribution of these inferred densities is shown in Figure 9. Note that, in fact, the densities we have derived are lower limits. They could be higher than this if part of the line width arises from turbulence, or if we have underestimated the ionizing flux.

Using the temperature and hydrogen ionization dependence on density (Fig. 8), it is possible to derive approximate sizes for the clouds from the observed H I column densities and velocity dispersions. In general these are in the range

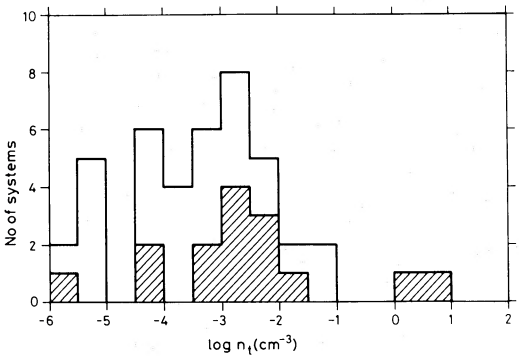


FIG. 9.—An inferred distribution of particle densities in the Lyα clouds, assuming that the line width is entirely thermal and the clouds are heated by the diffuse quasar background radiation. The shaded portions refer to lines apparently free from blending.

$3 \times 10^{18}$–$10^{22}$ cm. Thus the suggestion that the clouds should generally be larger than a typical quasar emission-line region ($10^{19}$ cm?) from the fact that the mean equivalent widths are the same for those absorptions in the Lyα emission line profile as in the continuum, appears to be consistent with these approximate results. However, there are some exceptionally small clouds. The most extreme case which is free from uncertainties due to blending is at $z_{\rm abs} = 1.90839$, where for the upper-limit velocity dispersion $b = 19$ km s$^{-1}$ the H I column density is $5.8 \times 10^{12}$ cm$^{-2}$ and the inferred size is about $6 \times 10^{17}$ cm. Another example of a small cloud on this model has been found in PHL 957 by Chaffee *et al.* (1983), who were the first to point out the difficulty in explaining large clouds with low velocity dispersions. On the basis of our data on Q1101−264, serious discrepancies of this sort are relatively unusual, especially if we consider the uncertainties in estimating the size of quasar emission-line regions. Thus it is still possible that we are seeing only the effects of a distribution of cloud sizes and densities. This is subject, of course, to the details of the model being correct, and particularly to the hope that we have not seriously overestimated the temperatures in the clouds or underestimated the ionizing background flux.

Note that the existence of a range of velocity dispersions, if they are predominantly thermal, argues against the possibility that both pressure confinement by an intergalactic medium and temperature equilibrium from quasar background heating are correct for these clouds. One constraint on the temperature is imposed by the assumption that a constant intergalactic pressure applies to all clouds at a given redshift, and so the temperature $T$ must be inversely proportional to the density $n_t$. For heating from the ionizing background radiation from quasars, Figure 8 shows that the temperature-density curve is, at its steepest, $T \propto n_t^{-0.3}$. Only one temperature (and hence velocity dispersion) will simultaneously satisfy these conditions, in contrast with the wide range of values found.

At our resolution we would easily be able to separate the D Lyα 1215.34 line from Lyα 1215.67 in any system in which they both occur. However, cosmologically significant values of the D/H ratio are expected to be less than $10^{-4}$ (Wagoner, Fowler, and Hoyle 1967; Pagel 1982), and our maximum H I column densities are too low by a factor of about 100 to expect a detection of deuterium. The Lyα line density is sufficiently high, though, that there is a good chance of systems being present with velocity separations of about 80 km s$^{-1}$, which will mimic a D/H separation. We find six of these, with the formal D/H number ratio ranging from 0.05 to 4. This suggests that, even if suitable high H I column density systems are found (Adams 1976 gives a description of the properties of suitable systems), the D/H ratio will be uncertain because of velocity structure. Either it will have to be established through a large sample of such systems that D/H always exceeds some value, or at best an upper limit will be possible.

## VI. CONCLUSIONS

High-resolution spectra of the quasar Q1101−264 have revealed that the $z_{\rm abs} = 1.8387$ system which Carswell *et al.* (1982), on the basis of 1.5 Å resolution spectra, reported as a single system, in fact consists of at least five velocity components. Internal inconsistencies in redshift and velocity dispersion suggest that there may be even more, and the difficulty in adequately modeling the clouds is also suggestive. The total velocity spread over this complex is 160 km s$^{-1}$.

A further absorption complex occurs at $z_{abs} = 0.359$. Here the total velocity spread is 630 km s$^{-1}$, which is rather high for a single galaxy but consistent with a cluster. This system appears to consist of two pairs of clouds, with separations within the pairs of order 25 and 40 km s$^{-1}$. CTIO 4 m plates of the field show a number of galaxies in this region of the sky, but the redshifts of the galaxies so far measured do not agree well with that of the absorption system. The closest galaxy redshift is about 2000 km s$^{-1}$ higher than that of the quasar absorption complex.

The lines in the Ly$\alpha$ forest have been resolved, and the velocity dispersions range from about 10 to 45 km s$^{-1}$. The lower end of the range is consistent with temperatures in the expected range $10^4 < T < 4 \times 10^4$ K, but higher velocity dispersions, corresponding to cloud temperatures greater than $10^5$ K, are not uncommon. It is likely that turbulence or bulk motions of some sort are responsible for these high values, since thermal and ionization equilibrium models suggest that $10^5$ K is about the maximum expected. The observed Ly$\alpha$ equivalent width distribution function is found to differ markedly from that reported by Sargent *et al.* (1980). We find, for rest equivalent width $W$ and a distribution of the form

$$p(W) \alpha \exp(-W/W^*),$$

$W^* = 0.16 \pm 0.02$ Å, in contrast with their $W^* = 0.36 \pm 0.02$ Å. The difference is probably the result of our considerably higher resolution. Estimates of the H I column density are not well fitted by an exponential law of this form. Over the observed range a power law provides an adequate fit, but it is clear that this breaks down for column densities $N(\text{H I}) < 10^{13}$ cm$^{-2}$.

There is weak evidence that the velocity dispersion in the Ly$\alpha$ lines is correlated with the H I column density as might be expected if, for example, the clouds are partially confined by self-gravity. The redshift two-point correlation function showed no significant peak on scales of greater than 50 km s$^{-1}$, and so it is consistent with there being no clustering of the clouds. The sample size is still small, however, and confirmation (or otherwise) of these results from larger samples is required. If the clouds are intergalactic and have primordial element abundances, then it is of cosmological interest to search for high H I column density systems where deuterium might be detected. The highest H I column density found here is too low ($10^{15}$ cm$^{-2}$) to be of interest, but there are several cases where the velocity difference between Ly$\alpha$ clouds mimicked the D-H separation. This likelihood in general will complicate future searches for deuterium.

We are grateful to John Graham for obtaining the Cerro Tololo 4 meter plates of the field, to Paul Murdin for allowing us to observe Q1101−264 during part of a night of his observing time, and to the AAO mountain staff who made it all possible. We thank Bernard Jones for useful discussions during the early stages of this investigation, and Gary Ferland for the use of his photoionization program. Much of the analysis software was developed on the Starlink computer in Cambridge, and we are grateful to the UK Science and Engineering Research Council for the provision of this facility. R. F. C. acknowledges support from the SERC and the Radcliffe Trust; R. J. W. acknowledges support from the National Science Foundation.

REFERENCES

Adams, T. F. 1976, *Astr. Ap.*, **50**, 461.
Arons, J., and Wingert, D. W. 1972, *Ap. J.*, **177**, 1.
Bahcall, J. N., and Wolf, R. A. 1968, *Ap. J.*, **152**, 701.
Black, J. H. 1981, *M.N.R.A.S.*, **197**, 553.
Boksenberg, A., and Snijders, M. A. J. 1981, *M.N.R.A.S.*, **194**, 353.
Carswell, R. F., Whelan, J. A. J., Smith, M. G., Boksenberg, A., and Tytler, D. 1982, *M.N.R.A.S.*, **198**, 91.
Chaffee, F. H., Weymann, R. J., Latham, D. W., Wyatt, W. F., and Field, G. B. 1982, *Bull. AAS*, **14**, 908.
Chaffee, F. H., Weymann, R. J., Latham, D. W., and Strittmatter, P. A. 1983, *Ap. J.*, **267**, 12.
de Boer, K. S., and Savage, B. D. 1980, *Ap. J.*, **238**, 86.
Dufton, P. L., Hibbert, A., Kingston, A. E., and Tully, J. A. 1982, preprint.
Kendall, M. G., and Stuart, A. 1967, *The Advanced Theory of Statistics*, Vol. **2** (London: Griffith).
Lampton, M., Margon, B., and Bowyer, S. 1976, *Ap. J.*, **208**, 177.
Melott, A. L. 1980, *Ap. J.*, **241**, 889.
Morton, D. C. 1978, *Ap. J.*, **222**, 863.
Osmer, P. S., and Smith, M. G. 1977, *Ap. J.*, **213**, 607.
Pagel, B. E. J. 1982, *Phil. Trans. R. Roc. London, A*, **307**, 19.
Pettini, M., and West, K. A. 1982, *Ap. J.*, **260**, 561.
Röser, H.-J. 1975, *Astr. Ap.*, **45**, 329.
Sargent, W. L. W., Young, P. J., Boksenberg, A., Carswell, R. F., and Whelan, J. A. J. 1979, *Ap. J.*, **230**, 49.
Sargent, W. L. W., Young, P. J., Boksenberg, A., and Tytler, D. 1980, *Ap. J. Suppl.*, **42**, 41.
Savage, B. D., and de Boer, K. S. 1979, *Ap. J. (Letters)*, **230**, L77.
Shull, J. M., Snow, T. P., and York, D. G. 1981, *Ap. J.*, **246**, 549.
Wagoner, R. V., Fowler, W. A., and Hoyle, F. 1967, *Ap. J.*, **148**, 3.
Weisheit, J. C., and Collins, L. A. 1976, *Ap. J.*, **210**, 299.
Weymann, R. J., Carswell, R. F., and Smith, M. G. 1981, *Ann. Rev. Astr. Ap.*, **19**, 41.
Weymann, R. J., Williams, R. E., Peterson, B. M., and Turnshek, D. A. 1979, *Ap. J.*, **234**, 33.
York, D. G. 1982, *Ann. Rev. Astr. Ap.*, **20**, 221.
Young, P. J., Sargent, W. L. W., and Boksenberg, A. 1982, *Ap. J. Suppl.*, **48**, 455.

ROBERT F. CARSWELL: Institute of Astronomy, Madingley Road, Cambridge CB3 0HA, England

DONALD C. MORTON: Anglo-Australian Observatory, P.O. Box 296, Epping, N.S.W. 2121, Australia

MALCOLM G. SMITH: Royal Observatory, Blackford Hill, Edinburgh EH9 3HJ, Scotland

ALAN N. STOCKTON: Institute for Astronomy, 2680 Woodlawn Drive, Honolulu, HI 96822

DAVID A. TURNSHEK: Department of Physics and Astronomy, University of Pittsburgh, Allen Hall, Pittsburgh, PA 15260

RAY J. WEYMANN: Steward Observatory, University of Arizona, Tucson, AZ 85721